Eur. Phys. J. B **52**, 297–303 (2006)
DOI: 10.1140/epjb/e2006-00296-4

THE EUROPEAN PHYSICAL JOURNAL B

Ferromagnetic resonance in arrays of highly anisotropic nanoparticles

A. Butera[a]

Centro Atómico Bariloche, Comisión Nacional de Energía Atómica, and Instituto Balseiro, Universidad Nacional de Cuyo, 8400 San Carlos de Bariloche, Río Negro, Argentina

Received 20 April 2006 / Received in final form 26 June 2006
Published online 31 July 2006 –

Abstract. We present in this study computational simulations of the ferromagnetic resonance response of magnetic nanoparticles with a uniaxial anisotropy considerably larger than the microwave excitation frequency (in field units). The particles are assumed to be randomly oriented in a two dimensional lattice, and are coupled by dipolar interactions through an effective demagnetization field, which is proportional to the packing fraction. We have included in the model fluctuations in the anisotropy field (H_K) and allowed variations in the demagnetizing field. We then analyzed the line shape and line intensity as a function of both fields. We have found that when H_K is increased the line shape changes drastically, with a structure of two lines appearing at high fields. The line intensity has a maximum when H_K equals the frequency gap and decreases considerably for larger values of the anisotropy. The effects of fluctuations in H_K and variations in the packing fraction have been also studied. Comparison with experimental data shows that the overall observed behavior is dominated by the particles with lower anisotropy.

PACS. 76.50.+g Ferromagnetic, antiferromagnetic, and ferrimagnetic resonances; spin-wave resonance – 75.30.Gw Magnetic anisotropy – 75.50.Tt Fine-particle systems; nanocrystalline materials – 75.75.+a Magnetic properties of nanostructures

1 Introduction

The technique of ferromagnetic resonance (FMR) has been widely used for over half a century for the characterization of magnetic ordered materials. This technique is especially useful to study samples of reduced dimensionality (e.g. small particles and thin films) because a relatively small amount of material is enough to obtain a good signal to noise ratio. From the analysis of the resonance field, the line width, and the overall line shape it is possible to obtain valuable information about the sample magnetization, g-value, anisotropies, and their distribution. Early works in single domain particles [1,2] showed the effects that anisotropy had on the line shape. A more recent work by Netzelmann [3] studied the FMR response of partially oriented particulate magnetic recording tapes, stressing the effect that the distribution of particle orientations have on the line shape. Other authors [4,5] studied the influence of thermal effects on the resonance spectrum in the low anisotropy limit. Interparticle interactions have been also shown to modify the absorption line shape [6].

In the last few years there has been considerably interest in self-assembled two dimensional ordered arrays of high anisotropy magnetic nanoparticles due to their potential applications as media for ultrahigh density magnetic recording. FePt [7], FePt-Ag and FePt-Au [8] particles that crystallize in the low anisotropy ($K \sim 10^6$ erg/cm^3 [7]) FCC phase, transform to the $L1_0$ tetragonal phase after proper annealing above 500 °C. This phase has a very large magnetocrystalline anisotropy constant ($K \sim 10^7$ erg/cm^3) which enhances the thermal barrier for thermal switching. A recent FMR study [9] of as-made (FCC phase) and partially ordered (mixture of FCC and $L1_0$ phases) FePt-Au self assembled nanoparticles suggested that the measured absorption originates in the low anisotropy FCC phase in both samples. It is therefore of interest to study the possibility of observing an FMR signal in a system of high anisotropy self-organized nanoparticles forming a film.

2 Model

We have assumed that the system is composed of N particles of magnetization M forming a two dimensional array as sketched in Figure 1 . The particles possess a uniaxial anisotropy of magnetocrystalline origin of magnitude K and the anisotropy easy axes are randomly distributed. Particle shape effects, which are not explicitly considered, could be included in this term. The dipolar interaction

[a] Also at Consejo Nacional de Investigaciones Científicas y Técnicas, Argentina; e-mail: butera@cab.cnea.gov.ar

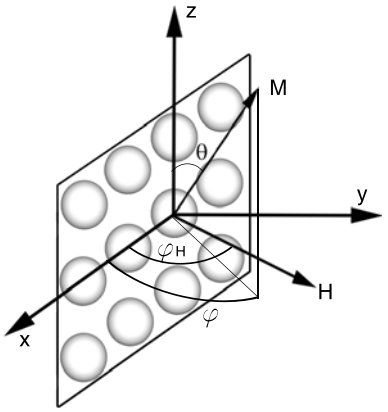

Fig. 1. Schematic drawing of the system under study. The particles lay on plane forming a two dimensional array. Each particle has a magnetization vector M with spherical angles θ and φ and a randomly oriented easy axis in a direction given by the angles θ_p and φ_p (not shown). The magnetic field H is rotated within the xy plane and forms an angle φ_H with the x-axis.

among particles is accounted through an effective magnetostatic energy which is a combination of the limiting cases of isolated particles and a thin film [3].

The magnetic free energy density per particle can then be written as:

$$F = -\mathbf{M}\cdot\mathbf{H} - \frac{K}{|M|^2}\left(\mathbf{M}\cdot\hat{\mathbf{n}}\right)^2 + \frac{1}{2}\mathbf{M}\cdot\mathbf{N}\cdot\mathbf{M}. \quad (1)$$

In this expression $\mathbf{H}$ is the external magnetic field, the versor $\hat{\mathbf{n}} = (\cos\varphi_p \sin\theta_p, \sin\varphi_p \sin\theta_p, \cos\theta_p)$ is a unit versor pointing in the direction of the particle easy axis, and the components of the effective demagnetization tensor $\mathbf{N}$ are (assuming that the film is placed in the xz plane) $N_{ij} = 4\pi P$ if $i = j = y$, $N_{ij} = 0$ otherwise. P is the packing fraction that tends to one for a continuous thin film and goes to zero for isolated particles. As the particles are assumed to be spherical, the additional demagnetizing term that should appear in equation (1) to fulfill the condition $\sum N_{ii} = 4\pi$, is isotropic and only adds a constant term that was omitted in the present analysis. The free energy can be also written as a function of the angular variables,

$$\begin{aligned} F = &-MH\sin\theta\cos(\varphi-\varphi_H) \\ &- K(\sin\theta\sin\theta_p\cos(\varphi-\varphi_p) + \cos\theta\cos\theta_p)^2 \\ &+ 2\pi P M^2 \sin^2\theta\sin^2\varphi, \end{aligned} \quad (2)$$

where θ and φ are the polar and azimuthal angles of the particle magnetization vector, and φ_H is the angle between the field $\mathbf{H}$ and the x-axis. For simplicity $\mathbf{H}$ is rotated in the xy plane (see Fig. 1).

In the present analysis we will consider only the case of particles which have an easy axis of anisotropy. We have explicitly written the negative sign in equations (1) and (2) in order to work with the absolute value of K throughout the paper. The case of positive anisotropy can be treated within the same theoretical framework by changing the sign of K, but the analysis of hard axis magnetic anisotropy is outside the scope of this work. Results in the limit of small K have been reported in references [4] and [5].

The dispersion relation can be obtained from the damped equation of motion, $\dot{\mathbf{M}} = -\gamma\left(\mathbf{M}\times\mathbf{H}\right) - \frac{\alpha\gamma}{M}\left(\mathbf{M}\times\left(\mathbf{M}\times\mathbf{H}\right)\right)$, using the Smit and Beljers formula [3,10]

$$\left(\frac{\omega}{\gamma}\right)^2 = \frac{1+\alpha^2}{M^2\sin^2\theta}\left(\frac{\partial^2 F}{\partial\theta^2}\frac{\partial^2 F}{\partial\varphi^2} - \frac{\partial^2 F}{\partial\theta\partial\varphi}\right) + \left(\frac{\Delta\omega}{\gamma}\right)^2, \quad (3)$$

$$\frac{\Delta\omega}{\gamma} = \frac{\alpha}{2M}\left(\frac{\partial^2 F}{\partial\theta^2} + \frac{1}{\sin^2\theta}\frac{\partial^2 F}{\partial\varphi^2}\right). \quad (4)$$

In the above equations $\alpha = G/(\gamma M)$ with G the phenomenological damping factor, and $\gamma = g\mu_\beta/\hbar$ ($g = 2.09$ for metallic Fe).

The scalar magnetic susceptibility (which gives the microwave response of the system to the microwave perturbation field) can be written as [1,3]:

$$\begin{aligned} \chi = \chi' + i\chi'' = &\frac{1+\alpha^2}{\left(\frac{\omega}{\gamma}\right)^2 + \left(i\frac{\omega_0}{\gamma} + \frac{\Delta\omega}{\gamma}\right)^2} \\ &\times\left[l^2\left(\frac{\partial^2 F}{\partial\theta^2} + i\alpha'\right) + m^2\left(\frac{1}{\sin^2\theta}\frac{\partial^2 F}{\partial\varphi^2} + i\alpha'\right)\right. \\ &\left. + 2lm\frac{\partial^2 F}{\partial\theta\partial\varphi}\frac{1}{\sin\theta}\right], \end{aligned} \quad (5)$$

with ω_0 the excitation microwave frequency, $\alpha' = \frac{\omega_0}{\gamma} M\frac{\alpha}{1+\alpha^2}$, and $l = 0$, $m = -\sin\theta$ when the microwave field is applied in the z direction (as assumed in the present case). The absorbed power is proportional to χ'', and hence the line shape can be written as:

$$\chi''(\omega) = \frac{\omega_0}{\gamma}\frac{\left(\frac{\Omega}{\gamma}\right)^2\alpha M\sin^2\theta - \left(1+\alpha^2\right)2\frac{\Delta\omega}{\gamma}\frac{\partial^2 F}{\partial\varphi^2}}{\left(\frac{\Omega}{\gamma}\right)^4 + \left(\frac{\omega_0}{\gamma}\frac{2\Delta\omega}{\gamma}\right)^2}, \quad (6)$$

and

$$\begin{aligned} \frac{\partial^2 F}{\partial\varphi^2} = &M\sin\theta\left[H\cos(\varphi-\varphi_H) + 4\pi M P\sin\theta\cos 2\varphi\right. \\ &+ H_K\sin\theta_p\left(\cos\theta_p\cos\theta\cos(\varphi-\varphi_p)\right. \\ &\left.\left. + \cos 2(\varphi-\varphi_p)\sin\theta_p\sin\theta\right)\right], \end{aligned} \quad (7)$$

with $H_K = 2K/M$ and $\left(\frac{\Omega}{\gamma}\right)^2 = (\omega/\gamma)^2 - (\omega_0/\gamma)^2 + (\Delta\omega/\gamma)^2$.

To obtain the average susceptibility it is necessary to integrate χ'' in the angular variables θ_p and φ_p (which are assumed to have a random distribution) and other parameters which could have a variation around an average value. Fluctuations in the anisotropy field H_K and the magnetization M (to a less extent) could be relatively

large because of the partial transformation from the FCC to the $L1_0$ phase. If we assume a Gaussian distribution for both magnitudes we can arrive to the following expression for the average susceptibility:

$$\left\langle \chi''\left(\omega_0, H, \varphi_H, \bar{H}_K, \bar{M}\right)\right\rangle = \frac{1}{C}\int_0^\infty \int_0^\infty \int_0^{2\pi} \int_0^{\pi} \chi''\left(\omega_0, H, \varphi_H, H_K, M, \varphi_p, \theta_p\right) \times \sin\theta_p d\theta_p d\varphi_p e^{-\frac{(H_K-\bar{H}_K)^2}{2\sigma^2_{H_K}}} dH_K e^{-\frac{(M-\bar{M})^2}{2\sigma^2_M}} dM. \quad (8)$$

C is the normalization constant obtained by fixing $\chi'' \equiv 1$, and $\bar{H}_K$ and $\bar{M}$ are the average values of the anisotropy field and the magnetization with dispersion σ_{H_K} and σ_M, respectively. In the general case the above integral must be solved numerically. The first step is to obtain the magnetization equilibrium angles θ and φ for a given set of the parameters $\left\{\varphi_p, \theta_p, \bar{H}_K, \sigma_{H_K}, \bar{M}, \sigma_M, H, \varphi_H, \omega_0\right\}$ in order to evaluate the dispersion relation (Eq. (3)) and the frequency line width (Eq. (4)). The integration in the four variables must be made for each value of H, which consumes a considerable computational time. Alternatively, it is possible to generate a set of random orientations for φ_p and θ_p, and Gaussian distributed values for $\bar{H}_K$ and $\bar{M}$, then calculate the line shape and finally average out all the evaluated spectra. We have chosen this last approach to simulate the FMR response. In most cases we have fixed the number of spectra at 20 000 because, in general, the addition of more spectra does not change considerably the average spectrum shape or its intensity. In the cases where the noise level was important, the number of calculated spectra was raised to 10^6. The initial field for each spectrum always started at 0 Oe and the maximum field was varied depending on the values of the parameters used in the simulation. This field was chosen large enough so that a negligible absorption was computed for fields above this value. When evaluating the spectra the total field span was divided in 700 steps.

3 Results

In all simulations we have used a damping factor $\alpha = 0.2$ which gives an intrinsic line width of $\Delta\omega_0/\gamma = \Delta H_i \sim$ 750 Oe, similar to what was measured in FePt-Au [9]. The magnetization $\bar{M}$ was fixed at 1000 emu/cm^3 which is lower that the M_s value of FCC ($M_s \sim 1030$ emu/cm^3) and $L1_0$ ($M_s \sim 1100$ emu/cm^3) FePt [11], but larger that the reduced magnetic moment of small particles ($M_s \sim 850$ emu/cm^3) [12]. Due to the small difference in the ordered and disordered phases we have not considered fluctuations in $\bar{M}$ in the present analysis, i.e. $\sigma_M = 0$. We have chosen an excitation frequency $\nu = 9.6$ GHz, coincident with the commonly used X-band.

3.1 Case $\sigma H_K = 0, P = 0$

In Figure 2 we show a set of absorption spectra $\chi''(\omega)$ calculated for different values of the anisotropy field ($0 \leq H_K \leq 10$ kOe) and zero dipolar interaction ($P = 0$). In this case all directions of the applied field with respect to the film plane (measured by the angle φ_H) are equivalent and the average spectrum is isotropic. The expected dispersion relation (Eq. (3)) for different values of H_K is shown in Figure 3. Each set of curves corresponds to H parallel and perpendicular to the particle easy axis. The dispersion curves for intermediate orientations between **H** and $\hat{\mathbf{n}}$ always lay within this two curves. Note that a frequency gap of magnitude H_K occurs at $H = 0$. When the anisotropy field is lower than the excitation frequency

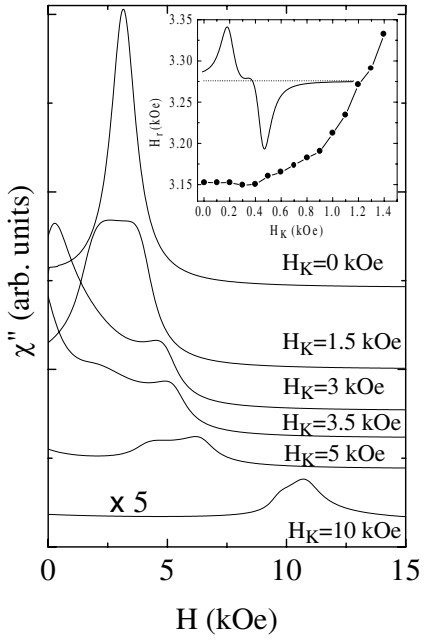

Fig. 2. Absorption spectra for different values of H_K, for the case $\sigma H_K = 0$, $P = 0$. Spectra have been shifted vertically for clarity. In the inset we show the variation of the resonance field as a function of the anisotropy field (for $H_K < 1.4$ kOe), and a spectrum derivative for $H_K = 1.4$ kOe.

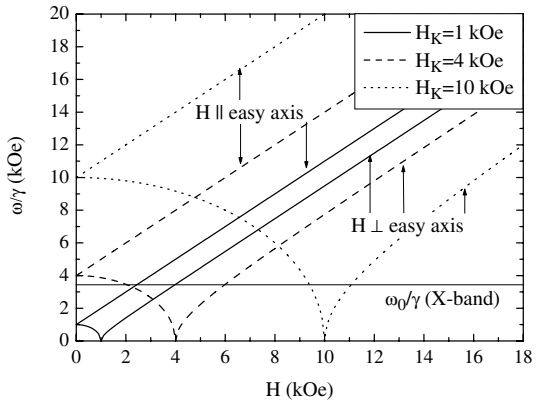

Fig. 3. ω/γ curves as a function of the applied field H for different values of H_K. Each set of curves corresponds to the particle easy axis oriented parallel (upper branch) or perpendicular (lower branch) to H. The resonance field is given by the intersections of these curves with the excitation frequency ω_0/γ.

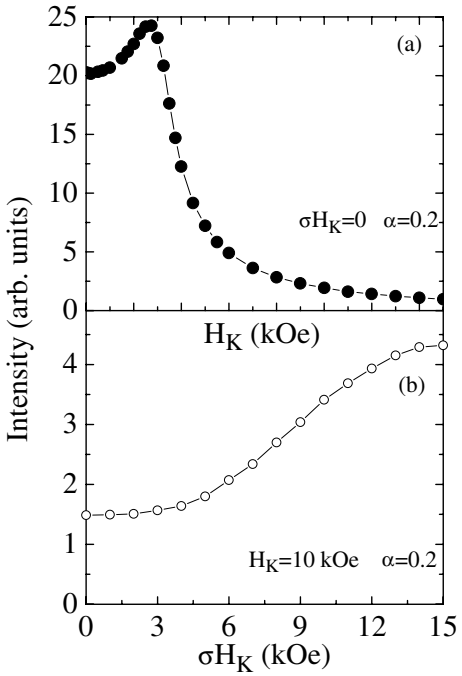

Fig. 4. (a) Variation of the line intensity as a function of the particle anisotropy field H_K. (b) Dependence of the line intensity with the dispersion in the anisotropy field σH_K for $H_K = 10$ kOe.

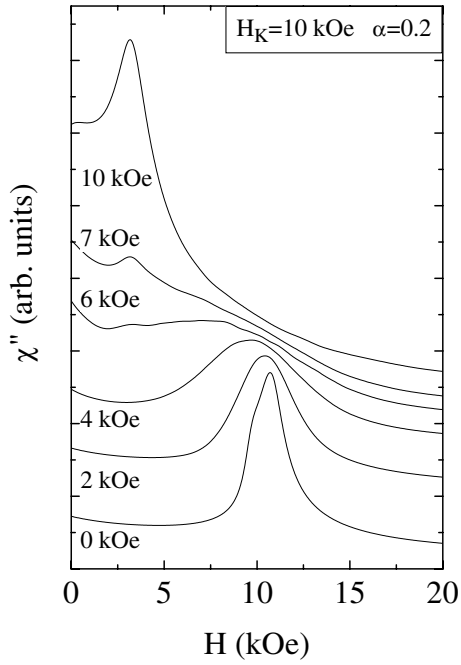

Fig. 5. Absorption spectra for different values of σH_K, for the case $\bar{H}_K = 10$ kOe, $P = 0$. Spectra have been shifted vertically for clarity.

(ω_0/γ) a single line is predicted for all particle orientations. If $H_K > \omega_0/\gamma$ the absorption can be observed only when the particle hard axis is close to the field H.

When H_K is much lower than ω_0/γ the influence of the anisotropy is minimal and all particle orientations are equivalent. Hence a single almost symmetrical line centered at $g = 2.09$ with a line width $\sim \Delta H_i$ is predicted. In this range of relatively low anisotropies the results are similar to those reported in references [4,5]. First, as shown in the inset of Figure 2, the resonance field (H_r is defined as the zero crossing of the spectrum derivative) gradually increases for larger anisotropy values (for values of $H_K > 1.4$ kOe the line derivative splits in two and the zero crossing criteria looses its validity). Second, in the absorption derivative the intensity of the high field part of the spectrum ($H > H_r$) is larger than the contribution for $H < H_r$ (see Fig. 2). When the anisotropy increases, the line broadens and a structure of two absorptions, one moving to low fields and the other to high fields is observed. Also the energy absorption at low fields increases considerably (see Fig. 2). For $H_K \sim \omega_0/\gamma$ the low field line crosses zero field and now the spectrum starts with a negative slope. The structure of two lines in a broad background is preserved, but now both lines move to high fields. When $H_K \gg \omega_0/\gamma$ only the particles with the easy axis perpendicular to the applied field fulfill the resonance condition. This implies (see Fig. 3) that two absorptions, each one corresponding to a different branch of the dispersion relation must be observed. Note that there is no contribution at low fields coming from particles that are not perpendicular to the external field.

It is of interest to study the behavior of the absorption intensity, defined as the field integral of the line shape, as a function of H_K. We can see in Figure 4a that initially the intensity tends to increase, it has a maximum when $H_K \lesssim \omega_0/\gamma$ and then decreases monotonically for larger H_K. This behavior can be understood looking at the variation of the line shape as a function of H for different values of the anisotropy (Fig. 2). Note that when H_K is approaching the value of the excitation frequency, the center of gravity of the spectrum moves to zero field, and the contribution from the symmetrical absorption occurring at negative fields becomes important. When $H_K > \omega_0/\gamma$ (but $\Delta\omega_0/\gamma \sim H_K - \omega_0/\gamma$) the dispersion relation again crosses the X-band frequency for a few orientations, but some absorption still occurs due to the intrinsic frequency line width $\Delta\omega_0$ being of the same order as the difference $H_K - \omega_0/\gamma$. In the case $H_K \gg \omega_0/\gamma$ the intensity of the spectra gradually goes to zero because in most orientations the resonance condition is not satisfied.

3.2 Case $\sigma H_K > 0$, $P = 0$

The assumption that the average value of H_K has zero dispersion is a very unrealistic one, especially in the case of FePt in which the transformation to the ordered phase is not complete when the annealing is made at temperatures below the order-disorder transition temperature. To study the effects of fluctuations in the value of the anisotropy we have assumed an average anisotropy field $\bar{H}_K = 10$ kOe, considerably larger than ω_0/γ, and varied σH_K from zero to 15 kOe. A number of representative spectra are shown in Figure 5. For small σH_K the maximum in the

absorption occurs close to $H \sim \bar{H}_K$. As already mentioned, when $\bar{H}_K$ is considerable larger than ω_0/γ a structure due to the two branches of the dispersion relation is observed. When the distribution of anisotropy fields increases, spectra with smaller and larger values than $\bar{H}_K$ are averaged. However, as was shown in Figure 4a, the intensity of the spectra is, in general, larger for smaller H_K. Hence the center of gravity of the average spectrum is expected to move to low fields when σH_K increases. When $\sigma H_K \gtrsim \bar{H}_K$ the peak in $\chi''(H)$ is found close to $g = 2.09$ (∼3000 Oe) and the relative maximum near $\bar{H}_K$ could be hardly observed. Note that the peak to peak line width of the derivative of this line is $\Delta H \sim 1100$ Oe, i.e. of the same order as the intrinsic line width.

It is also possible to evaluate the line intensity (see Fig. 4b) to verify that as σH_K increases the contribution of the particles with smaller anisotropy becomes more important and the average line intensity tends to increase.

3.3 Case $\sigma H_K = 0$, $P > 0$

The simplest approach to account for the effects of dipolar interactions in a collection of particles is to introduce a packing fraction P. In self assembled arrays the particles form a two dimensional film and it is assumed that the effective demagnetizing field of a thin film could be expressed as $4\pi PM$. All previous simulations were made considering that the particles did not interact, and P was set equal to zero. In real FePt samples the packing fraction was estimated as [9] $P \sim 0.2$ (from TEM micrographs) and then a nonzero demagnetizing field is expected to change the magnetic response, depending on the relative orientation between the magnetic field and the film plane.

For the simulations we have chosen an average anisotropy field $\bar{H}_K = 10$ kOe, larger than the working frequency, and analyzed the cases $4\pi PM < \bar{H}_K$ and $4\pi PM > \bar{H}_K$, for $\sigma H_K = 0$, 5, and 10 kOe. All other parameters were not changed from those used in the previous simulations.

In the case $\sigma H_K = 0$, $P \ll 1$ the simulations predict, as expected, a single line (with a small structure) that resonates at lower fields when $\varphi_H = 0$ (H parallel to the film plane) and moves to larger fields for $\varphi_H = 90°$ (see the upper panel of Fig. 6). The field separation between the maxima in these two orientations is of the order of $4\pi PM$ (this holds only when P is small enough). As P is increased the field separation between the maxima increases and the lines broaden, particularly for $\varphi_H = 0$. For $P = 0.5$ the parallel absorption has a structure of two superimposed lines, while the perpendicular line moves to larger fields without changing considerably the overall shape. When $P = 1$ the demagnetizing field $4\pi M > \bar{H}_K$. In this case the parallel absorption peaks close to zero field, while preserving the structure of two maxima in a decreasing background. All the behavior previously described is a consequence of the contribution of the last term in equation (2). This term is responsible for the very large anisotropy observed when moving the applied field out of plane; and changes the dispersion relation in such a way that only minor changes occur in the shape of the perpendicular absorption when P is increased. The shape of the parallel absorption, on the other hand, has a strong dependence on the packing fraction.

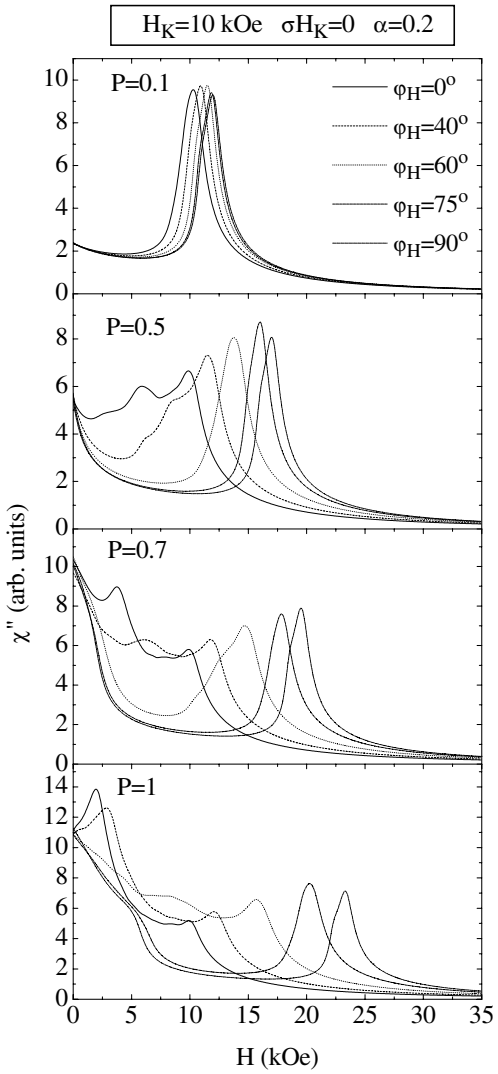

Fig. 6. Absorption spectra for different values of P and φ_H, for the case $\bar{H}_K = 10$ kOe, $\sigma H_K = 0$.

3.4 Case $\sigma H_K > 0$, $P > 0$

We have also studied the cases in which a non-zero dispersion in the anisotropy field is present. In the case $\sigma H_K = 5$ kOe the major effect of the fluctuations is to broaden the absorptions and to move the resonance fields to lower values. Also a broad decreasing background starting at zero field is predicted for all orientations. When the fluctuations in the anisotropy field are increased to $\sigma H_K = 10$ kOe the lines move to even lower fields, approaching $g = 2.09$ as discussed in the previous section. The broad background also increases, but the line width seems to diminish, as can be seen in Figure 7 for the case $P = 0.1$.

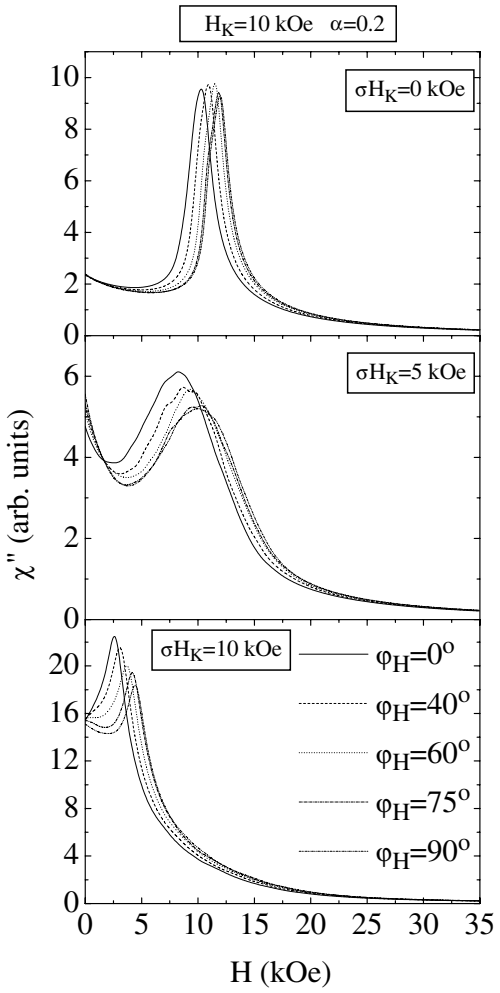

Fig. 7. Absorption spectra for different values of φ_H, for the case $P = 0.1$, $\bar{H}_K = 10$ kOe, $\sigma H_K = 0$, 5, and 10 kOe.

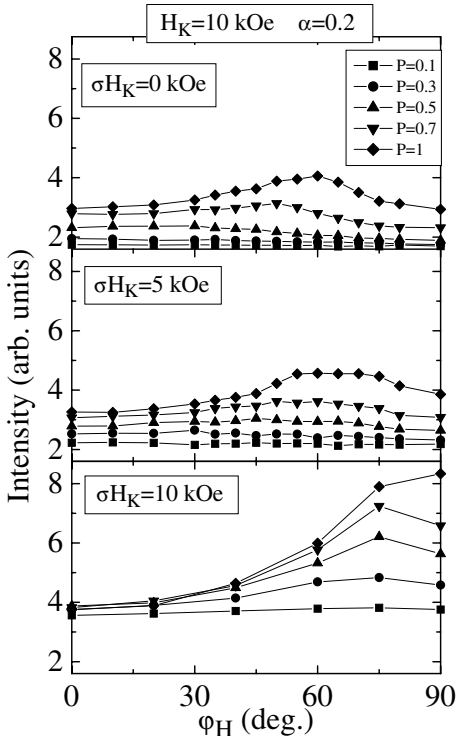

Fig. 8. Absorption intensity as a function of the field angle φ_H for $\bar{H}_K = 10$ kOe, $\sigma H_K = 0$, 5, and 10 kOe and different values of P.

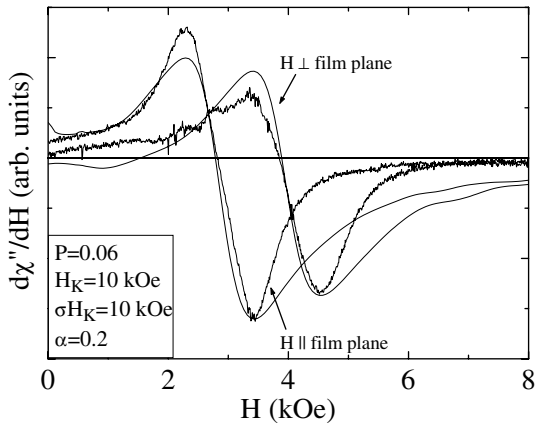

Fig. 9. Experimental spectra measured parallel and perpendicular to the film plane and predicted line shape from the proposed model.

In this case it is also possible to study the variations in line intensity as a function of P, σH_K, and φ_H. In Figure 8 we can see that in all angular variations the intensity increases for larger P. This behavior can be also observed in Figure 6 where the increasing absorption, particularly at low fields, accounts for the additional intensity. The origin of this behavior resides in the combination of an easy plane anisotropy (given by the effective demagnetization field $4\pi PM$) which tends to lower the energy gap, and a random oriented easy axis. In general, a dispersion relation with an easy plane anisotropy has a zero frequency gap and hence the intensity is larger because the average energy gap tends to be lower.

3.5 FMR absorption in FePt-Au particles.

In Figure 9 we show the room temperature FMR spectra of an FePt-Au sample that was already characterized in reference [9]. This sample was annealed at 450 °C for 30 minutes so that the transformation to the high anisotropy $L1_0$ phase was not complete. The two spectra correspond to the film plane oriented parallel and perpendicular to the external dc field. We have tried to fit these absorptions with the model presented above, assuming that both the low anisotropy FCC and the $L1_0$ phase contribute to the observed line shape through an average anisotropy field, with a relatively large dispersion. In Figure 9 we also show the spectra obtained by assuming the following values for the parameters: $P = 0.06$, $\bar{H}_K = 10$ kOe, $\sigma H_K = 10$ kOe, and $\alpha = 0.2$. Note that while it is possible to obtain reasonable good values for the resonance field, the line width,

and the relative intensity between both lines, the tail at high fields goes to zero much slower in the simulations than in the real spectra. This is a consequence of the broad background absorption produced by the large Gaussian distribution of anisotropy fields assumed in the simulations (see upper curve of Fig. 5). The relatively sharp and symmetric absorptions that are observed experimentally suggest that the distribution of anisotropy fields is not very large and that the average anisotropy field should be close to the value expected for the disordered FCC phase. Hence the assumption of a Gaussian distribution around an intermediate average value is not adequate in this particular case because the sample probably consists of different regions with ordered and disordered particles.

In conclusion, we have extensively analyzed the microwave response of a collection of high anisotropy magnetic nanoparticles, as a function of the anisotropy, the distribution of anisotropy fields and the packing fraction. We have shown that the experimental spectra observed in partially ordered FePt-Au films arise mainly in the low anisotropy disordered phase.

We wish to acknowledge the financial support of ANPCyT through grant PICT 03-13297, Conicet through grant PIP 5250, and the University of Cuyo. Very helpful discussions with C.A. Ramos and E. De Biasi are greatly acknowledged.

References

1. E.P. Valstyn, J.P. Hanton, A.H. Morrish, Phys. Rev. **128**, 2078 (1962)
2. K.A. Hempel, Z. Angew. Physik **28**, 280 (1970)
3. U. Netzelmann, J. Appl. Phys. **68**, 1800 (1990)
4. E. de Biasi, C.A. Ramos, R.D. Zysler, J. Magn. Magn. Mat. **262**, 235 (2003)
5. Yu L. Raikher, V.I. Stepanov, Sov. Phys. JETP **75**, 764 (1992)
6. I. Dumitru, D.D. Sandu, C.G. Verdes, Phys. Rev. B **66**, 104432 (2002); C.G. Verdes, B. Ruiz-Diaz, S.M. Thompson, R.W. Chantrell, I. Stancu. J. Appl. Phys. **89**, 7475 (2001)
7. S. Sun, C.B. Murray, D. Weller, L. Folks, A. Moser, Science **287**, 1989 (2000)
8. S. Kang, J.W. Harrell, D.E. Nickles, Nano Lett. **2**, 1033 (2002); S.S. Kang, D.E. Nickles, J.W. Harrell, J. Appl. Phys. **93**, 7178 (2003); S. Kang, Z. Jia, D.E. Nickles, J.W. Harrell, IEEE Trans. Magn. **39**, 2753 (2003)
9. A. Butera, S.S. Kang, D.E. Nikles, J.W. Harrell, Physica B **354**, 108 (2004)
10. J. Smit, H.G. Beljers, Philips Res. Rep. **10**, 113 (1955)
11. G.A. Held, Hao Zeng, Shouheng Sun, J. Appl. Phys. **95**, 1481 (2004)
12. X.W. Wu, C. Liu, L. Li, P. Jones, R.W. Chantrell, D. Weller, J. Appl. Phys. **95**, 6810 (2004)